Shadow electrochemiluminescence imaging of giant liposomes opening at polarized electrodes

Fatma Ben Trad, Jérôme Delacotte, Frédéric Lemaître, Manon Guille-Collignon, Stéphane Arbault, Neso Sojic, Eric Labbé, Olivier Buriez

ARTICLE

Shadow electrochemiluminescence imaging of giant liposomes opening at polarized electrodes

Received 00th January 20xx,
Accepted 00th January 20xx

DOI: 10.1039/x0xx00000x

Fatma Ben Trad,[a] Jérôme Delacotte,[a] Frédéric Lemaître,[a] Manon Guille-Collignon,[a] Stéphane Arbault,[b] Neso Sojic,[c]* Eric Labbé [a] and Olivier Buriez [a]*

In this work, the release of giant liposomes (~ 100 µm in diameter) content was imaged by shadow electrochemiluminescence (ECL) microscopy. Giant unilamellar liposomes were pre-loaded with a sucrose solution and allowed to sediment at an ITO electrode surface immersed in a solution containing a luminophore ($[Ru(bpy)_3]^{2+}$) and a sacrificial co-reactant (tri-*n*-propylamine). Upon polarization, the electrode exhibited illumination over its entire surface thanks to the oxidation of ECL reagents. However, as soon as liposomes reached the electrode surface, dark spots appeared then spread over time on the surface. This observation reflected a blockage of the electrode surface at the contact point between the liposome and the electrode surface, followed by dilution of ECL reagents after rupture of the liposome membrane and release of its internal ECL-inactive solution. Interestingly, ECL reappeared in areas where it initially faded, indicating back-diffusion of ECL reagents towards the previously diluted area and thus confirming liposome permeabilization. The whole process was analyzed qualitatively and quantitatively within the defined region of interest. Two mass transport regimes were identified: a gravity-driven spreading process when the liposome releases its content leading to ECL vanishing and a diffusive regime when ECL recovers. The reported shadow ECL microscopy should find promising applications for the imaging of transient events such as molecular species released by artificial or biological vesicles.

Introduction

Lipid membranes permeability is an important feature of natural membranes. It is a fundamental feature to control the passage of molecular species and ions from inside or outside living cells. This physiologically required permeation is achieved either actively by membrane transport proteins and channels, or by passive diffusion.[1] Moreover, this property can be used to control the administration of molecules such as for drug delivery. In this case, several strategies have been developed to increase membrane permeability:[2] (i) by directly acting on the membrane integrity, through electroporation or by using either specific radiations or biomolecules (e.g. Cell Penetrating Peptides, CPPs, or AntiMicrobial Peptides, AMPs),[3] or (ii) indirectly, by varying some physico-chemical properties of the medium (pH, temperature, ionic force) or by adding organic solvents.[2]

Within this framework, various analytical approaches based on either fluorescence, electrochemical or electrophysiological techniques have been implemented to characterize and study in real time the flow of molecules released from, or crossing, natural or artificial membranes. For instance, non-faradaic electrical techniques (e.g. "patch-clamp") are widely used to investigate ionic currents in individual living cells, single channels, or patches of cell membranes.[4] Optical techniques such as fluorescence are also widespread approaches, provided fluorescent markers are used.[5] Similarly, electrochemical strategies are relevant in the presence of redox molecules not only to detect and quantify them, but also to image cells.[6] For instance, amperometry is a powerful approach to locally detect and quantify molecular species secreted by living cells[7] or crossing lipid membranes.[8, 9] In this context, fluorescence modulation of organic fluorescent or fluorogenic molecules can also be electrochemically-triggered.[10-12] Accordingly, electrochemical quenching of the fluorescence produced by NBD-labelled cell penetrating peptides allowed investigation of their internalization in large unilamellar vesicles (LUVs).[13] In another relevant example, a dual functional electroactive and fluorescent probe was used for coupled measurements of vesicular exocytosis with high spatial and temporal resolution.[14]

Recently, we developed an original approach based on electrogenerated chemiluminescence (also called electrochemiluminescence, ECL)[15, 16] allowing to image liposome permeabilization processes triggered either by electroporation[17] or by the presence of the melittin AMP,[18] an anti-microbial peptide. On the one hand, liposomes (i.e., vesicles composed of a

[a] PASTEUR, Département de Chimie, Ecole Normale Supérieure, PSL University, Sorbonne Université, CNRS, 75005 Paris, France.
[b] Univ. Bordeaux, CNRS, Bordeaux INP, CBMN, UMR 5248, F-33600 Pessac, France.
[c] Univ. Bordeaux, CNRS, Bordeaux INP, ISM, UMR 5255 CNRS, 33400 Talence, France.

† Footnotes relating to the title and/or authors should appear here.
Electronic Supplementary Information (ESI) available: [details of any supplementary information available should be included here]. See DOI: 10.1039/x0xx00000x

phospholipid bilayer) are widely investigated due to their increasing interest not only in active and passive lipid barrier crossings, but also in fields as diverse as targeted drug delivery,[19-21] bioreactors,[22-24] membrane protein science,[25-27] and artificial cells.[28-37] On the other hand, ECL is a light-emitting phenomenon triggered by an initial electrochemical reaction occurring at an electrode surface. Compared to fluorescence, ECL provides higher sensitivity due to the absence of incident light.[38, 39] Thus, numerous immunoassays and clinical diagnosis are now performed by ECL.[40-44] In addition, it was demonstrated that ECL can be performed under microscopy[45-50] allowing to image single micro- and nano-objects,[51-58] especially of biological interest.[59-70]

In the most common ECL approach, the $[Ru(bpy)_3]^{2+}$ luminophore is used in combination with the tri-*n*-propylamine (TPrA) co-reactant. This system has been developed in two main imaging configurations: (i) "positive" ECL[54, 71-76] and (ii) "shadow" or "negative" ECL[53, 77-79]. In positive ECL microscopy configurations, the object of interest generates ECL light on dark background.[56, 65, 80] The ruthenium complex can be directly oxidized at the surface of interest or at a conductive surface placed in the vicinity of the object. In these examples, oxidation of either the luminophore or the co-reactant, or both, leads to an excited state of the ruthenium complex that emits a photon along its relaxation. In the shadow ECL (SECL) approach, the ECL reagents are freely diffusing in the medium containing the object of interest generating background ECL.[55, 79] Under this configuration the object blocks the electrode surface thus preventing any electron transfer. Therefore, no light can be produced at the place where the object is lying, thus exhibiting "negative" illumination in contrast with object-free areas which remain illuminated. This approach was especially used to image latent fingerprints, cells or mitochondria.[53, 77, 79, 81-83]

Interestingly, an ECL shadow phenomenon was also observed during a recent work dealing with the positive ECL imaging of the permeabilization of liposomes in which ECL reagents were formerly encapsulated.[17] In this case, a circular dark zone surrounded by ECL light was observed only during permeabilization of the liposome membrane that was triggered by the electrode polarization (before permeabilization, the image was totally dark). Under these conditions, (i.e., during permeabilization) the dark central area was ascribed to the contact point between the liposome and the electrode surface, where no electron transfer can occur, while the surrounding bright area accounted for the oxidation of ECL reagents released by the permeabilized liposome. On the basis of our previous experimental observations,[17] we extent such a view and describe herein the imaging of membrane permeabilization of giant liposome membranes using a negative optical contrast, that is a "negative ECL" or SECL. Compared with our recent positive ECL approach, SECL does not require the ECL reagents to be encapsulated inside liposomes. Moreover, considering the instability of DOPG membranes when in contact with TPrA,[17] liposomes prepared in the present work were made of DOPC (1,2-dioleolyl-*sn*-glycero-3-phosphocholine) phospholipids on their inner and outer leaflets. DOPC is a common phospholipid used in membrane permeability investigations notably in the presence of peptides.[3] Under these conditions, and as long as the liposome remains intact, a positive ECL light should be produced around a circular dark area corresponding to the contact point between the liposome and the electrode surface (Fig. 1). However, as soon as the membrane begins to be permeabilized under the electrode polarization effect, the dark zone should expand on the electrode surface upon dilution of the ECL reagents by the release of the encapsulated solution. Importantly, the presence of sucrose inside liposomes (whereas glucose is used outside liposomes) not only allowed their sedimentation towards the electrode surface (sucrose has a higher density than glucose), but also generated a gravity-driven spreading of the intra-liposomal solution on the electrode surface. Accordingly, the whole process was further evidenced by measuring the rate at which the black spot expanded, under pure diffusion or mixed with convection of the vesicles surrounding medium.

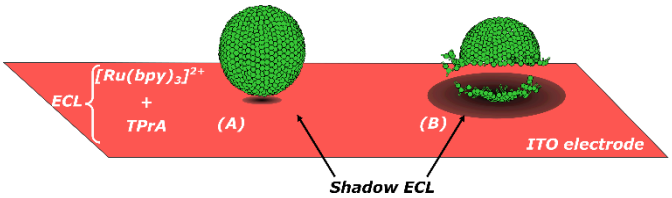

Fig. 1 Shadow ECL (SECL) imaging of a single giant liposome opening made of DOPC phospholipids and containing a sucrose solution (no ECL reagents), enabling its sedimentation. (A) Before liposome opening, the light is generated upon oxidation of ECL reagents freely diffusing around the liposome, but not at the contact point of the liposome with the electrode surface. (B) In case of membrane permeabilization (caused by the electrode polarization), the dark zone expands over time on the electrode surface due to dilution of the ECL reagents by the release of the internal ECL-inactive solution.

Experimental

Reagents

Tris(2,2'-bipyridyl)dichlororuthenium(II) hexahydrate, mineral oil, tri-*n*-propylamine (TPrA), D-(+)-glucose, sucrose, and phosphate buffer saline (PBS) tablets were purchased from Sigma Aldrich and used as received. Lipids: 1,2-dioleolyl-sn-glycero-3-phosphocholine (DOPC, 10 $mg.mL^{-1}$ in chloroform) were purchased from Avanti Polar. Water used for the preparation of extra- and intra-vesicular solutions was highly purified (resistivity=18 MΩ.cm; Milli-Q system; Millipore, Billerica, MA, USA).

Instrumentations

SECL experiments were carried out using a µAUTOLAB Type III connected to an electrochemical cell. The luminescent signals were collected by an EMCCD camera (Hamamatsu, Japan) connected to an inverted Zeiss (Axio Observer) microscope placed inside a Faraday cage as described elsewhere.[17]

Aqueous solutions

The intra-vesicular solution was made of sucrose (0.7 mol/L) dissolved in PBS (10 mmol/L, pH = 7.4). The PBS extra-vesicular solution contained glucose (0.7 mol/L; 1000 mOsm.kg^{-1}), TPrA (20 x 10^{-3} mol/L) and the ruthenium complex (30 x 10^{-6} mol/L). The pH value of this solution was adjusted to 7 by addition of phosphoric acid. The osmolality of freshly prepared intra-vesicular solutions was possibly adjusted at around 1000 mOsm.kg^{-1} by addition of PBS solution.

Phospholipid solutions

They were prepared as follows: 121 µL of a DOPC solution (10 mg.mL^{-1} in chloroform) was placed under vacuum for 2 hours to evaporate chloroform. Dried phospholipids were dissolved in mineral oil (2 mL) then sonicated (1 hour) to ensure complete dissolution.

Preparation of giant liposomes

As described elsewhere,[17] they were prepared in two steps. The first one consisted in the preparation of water in oil droplets surrounded by a monolayer of DOPC and containing the intra-vesicular solution. Then, droplets were passed through a water/oil interface containing DOPC phospholipids to form the liposome outer leaflets.

ITO microelectrodes

The transparent and conductive microelectrodes were made of ITO (150 nm-thick ITO films made of 90% In_2O_3/10% SnO_2, ACM, Villiers Saint Frédéric, France) deposited on optical glass slides (22 mm × 22 mm × 0.13 mm). The electrode surface (~ 800 µm in diameter) was delimited by a 1 mL pipette tip, playing the role of the electrochemical cell and inserted vertically in the PDMS well. A more detailed device description can be found in reference.[17]

ECL experiments

ECL was generated by applying a constant potential value of + 1.2 V *vs*. Ag/AgCl (used as the reference electrode) at the ITO working electrode. The counter electrode was a 1 cm length platinum wire. The quality of luminescent images could be optimized by the adjustment of the gain, and the exposure time (250 ms was a typical exposure time). Image analysis was performed using ImageJ software.[84]

Results and discussion

Positive ECL imaging of an ITO electrode surface in the absence of liposomes

First, we investigated the experimental conditions required to obtain a strong and stable ECL emission with the model ECL system (i.e., the $[Ru(bpy)_3]^{2+}$ luminophore and the TPrA co-reactant) at a conductive and transparent electrode (ITO). As shown in Fig. 2, an ECL signal was generated at the ITO electrode surface when polarized at + 1.2 V *vs*. Ag/AgCl. At this anodic potential, both ECL reagents are oxidized and the electrode generates homogeneous light over its entire surface.[17] From a quantitative point of view, Fig. 2 shows that the ECL intensity generated at the electrode surface increased very sharply and instantaneously as soon as the electrode was under polarization (see at around *t* = 10 s), then decreased slowly, proportionally to $1/t^{1/2}$, in agreement with a diffusion-controlled replenishment of the depleted zone. Such light intensity decay as a function of time and of the electrode polarization (Off *vs*. On) follows the evolution of a chronoamperometry experiment, with the advantage of allowing quantification of the process from luminescent images obtained by microscopy. As already investigated, light emission is restricted to a distance lower than 10 µm from the electrode, and is related to the diffusion rate and stability of the electrogenerated TPrA radicals ($t_{1/2}$ ~ 700 µs over distances greater than 1 µm with a diffusion coefficient D = 7.4 x 10^{-6} cm^2. s^{-1}).[80, 85-88]

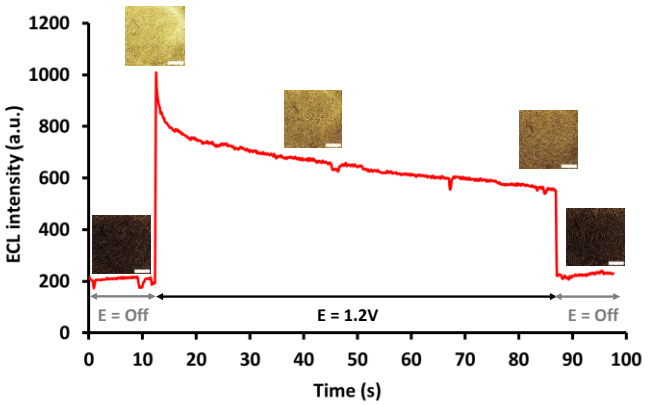

Fig. 2 ECL intensity and corresponding images (scale bare: 200 µm) were recorded on a microscope as a function of time at an ITO electrode surface (0.8 mm in diameter) immersed in a PBS solution (10^{-2} mol/L; pH = 7.54) containing $[Ru(bpy)_3]^{2+}$ (30 x 10^{-6} mol/L) and TPrA (20 x 10^{-3} mol/L). The potential value (+ 1.2 V vs. Ag/AgCl) was applied for approximately 75 seconds.

Shadow ECL (SECL) imaging of liposomes opening at a polarized ITO electrode surface.

After measuring the presence of ECL upon polarization of an ITO electrode, giant liposomes were added at the top of the electrochemical cell and let to sediment towards the electrode surface polarized at + 1.2 V *vs*. Ag/AgCl. Giant liposomes (100 µm in diameter) were made of DOPC on outer and inner leaflets and contained a sucrose solution (0.7 mol/L) to enable their sedimentation (sucrose has a higher density than glucose). Interestingly, and as a representative example, the images recorded at *t* = 120, 191 then 450 seconds (Fig. 3), clearly show a decrease in light intensity at different regions indicating that several liposomes reached the electrode surface.

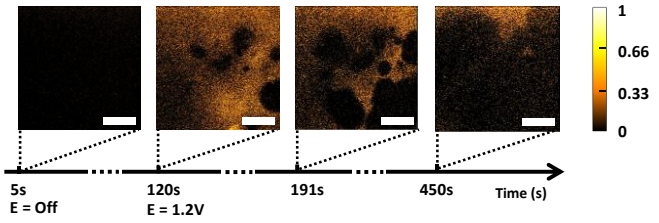

Fig. 3 Time-lapse imaging by shadow ECL showing the permeabilization of DOPC liposomes coming into contact with the surface of an ITO electrode polarized at + 1.2 V vs. Ag/AgCl from t = 120 s whereas liposomes were added in the electrochemical cell at t = 0 s. Liposomes containing sucrose (0.7 mol/L) were let to sediment in a solution containing $[Ru(bpy)_3]^{2+}$ (30 x 10^{-6} mol/L), TPrA (20 x 10^{-3} mol/L) and glucose (0.7 mol/L) dissolved in a PBS solution (10^{-2} mol/L; pH = 7.54). Scale bar: 200 µm.

More precisely, the image taken at *t* = 120 s and 191 s clearly shows the presence of circular dark areas whose diameters are larger than dark spots corresponding to the contact points between intact liposomes and the electrode surface. As shown in the video S1, corresponding to the right-hand corner of images shown in Fig. 3, a small circular dark zone first appears as soon as a liposome is in contact with the electrode surface, thus blocking any electron transfer at this point and consequently preventing electrochemically-triggered light emission. Then, and compared to our previous positive ECL investigations,[17] the dark spot spreads over time on the polarized electrode surface indicating liposome membrane permeabilization leading to a dilution of the ECL reagents present in the vicinity of the leaking zone(s). At this stage it is important to note that the spreading of the contents of a 100 µm diameter liposome over a 10 µm thick layer (active thickness in ECL) corresponds to an area 250 µm in diameter, which is the maximum diameter of the dark spot observed at *t* = 191 s. Finally, in a third phase, ECL reappeared in areas where it initially faded, indicating back-diffusion of ECL reagents towards the previously diluted area. However, the final dark zone remained larger than its initial size (i.e., the one corresponding to the contact point between the electrode and the intact liposome). Indeed, after membrane rupture, the electrode is blocked over a larger surface area due to the presence of phospholipids spread around the initial contact point between the liposome and the electrode. Accordingly, at longer times (*t* = 450 s), the electrode surface is almost completely dark, accounting for the combined contribution of ECL reagents dilution and phospholipid coating of the electrode surface.

Following this global observation, images obtained in the previous experiment and shown in Fig. 3 were restricted to the level of an isolated liposome (the one at bottom right of the image recorded at *t* = 120 s) to carry out a deeper qualitative study (Fig. 4). Fig. 4(A) shows a series of images obtained from the same experiment as that shown in Fig. 3 (see also the video in S.I.), but focused on an area of the electrode where a single liposome was deposited (see the dashed white circle in Fig. 4(A)). Compared with the previous global analysis of the whole electrode surface, the focus on a single liposome event provided additional relevant information. Firstly, and from a qualitative point of view, the arrival of a liposome on the electrode surface (before it comes into contact with the electrode surface) results in an increase in ECL intensity (compare the light intensity in images recorded at *t* = 30 s and *t* = 70 s). This increase can be explained by a local increase of ECL reagents concentrations consecutive to convection in the solution caused by the arrival of the investigated liposome in the studied zone. Of course, this phenomenon disappeared as soon as the liposome reached the electrode surface, resulting in the appearance of a black spot. As previously observed, the size of this spot became larger than the area of contact between the liposome and the electrode (see the image at *t* = 85 s in Fig. 4(A)), underlining the dilution of the ECL reagents following permeabilization of the liposome membrane and release of its ECL-inactive content. Interestingly, the image recorded several seconds later (see the image at *t* = 110 s) clearly shows ECL recovery in the area where it was extinguished (compare with the image taken at *t* = 70 s). This phenomenon indicates a diffusion of ECL reagents towards the previously diluted zone, confirming liposome permeabilization. However, the dark spot did not return to its original size (it remained larger) since phospholipids spread out around the initial contact point between the electrode and the liposome after membrane rupture of the latter, assessing thus the blocking character discussed above. At this stage, it is noteworthy to note that liposome electroporation starts stochastically at various times for different liposomes. Indeed, this process depends on the contribution of many experimental conditions (e.g. temperature, ionic strength, presence of defects in the lipid bilayer membrane, etc…) among which the contact surface between the liposome and the electrode is an important one. This contact surface will depend on the size of the liposome and the presence or absence of other liposomes in the vicinity.

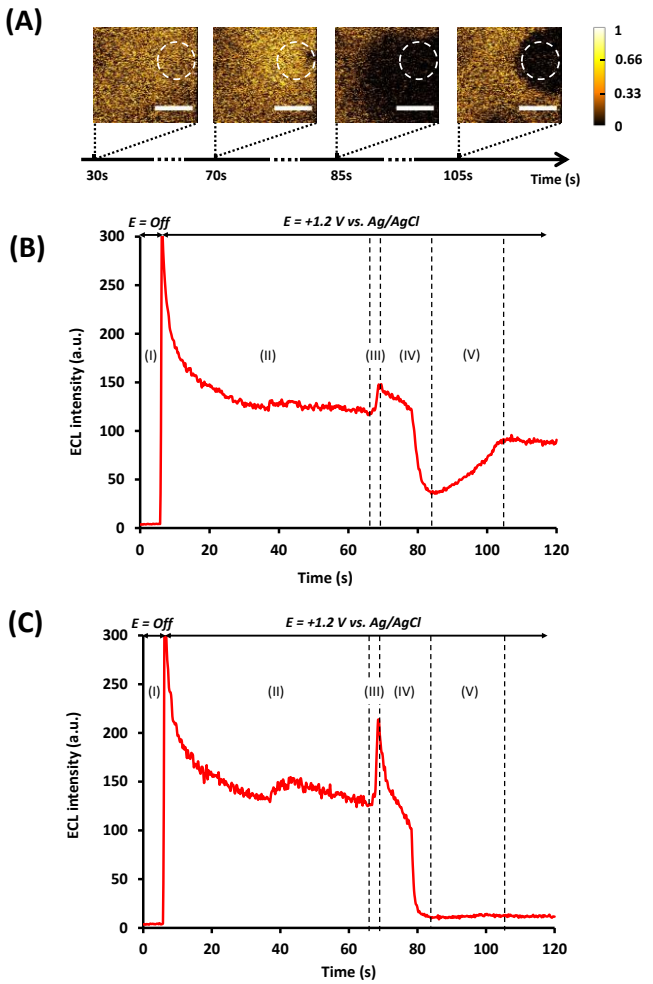

Fig 4 (A) Time-lapse imaging by shadow ECL showing the permeabilization of a DOPC liposome coming into contact with the surface of an ITO electrode polarized at + 1.2 V vs. Ag/AgCl. Liposomes containing sucrose (0.7 mol/L) were let to sediment in a solution containing $[Ru(bpy)_3]^{2+}$ (30 x 10^{-6} mol/L), TPrA (20 x 10^{-3} mol/L) and glucose (0.7 mol/L) dissolved in a PBS solution (10^{-2} mol/L; pH = 7.54). Scale bar: 100 µm. (B) - (C) Evolution of the ECL signal obtained as a function of time for a single liposome over a region of interest (ROI) which is (B) the whole image or (C) only the dashed white circle.

These qualitative analyses carried out from images shown in Fig. 4(A) were pushed further to gain more quantitative information, taking as region of interest either the entire image (Fig. 4(B)), or the liposome surrounded by the white dotted circle (Fig. 4(C)).

In the first case (Fig. 4(B)), the evolution of ECL intensity for the entire image follows perfectly the qualitative description discussed previously: the ECL intensity was zero when the potential was off (first few seconds; see (I) in Fig. 4(B)), but increased abruptly as soon as a potential value of + 1.2 V was applied. Under these conditions, and as observed in Fig. 2, the ECL then decreased up to 70 seconds proportionally to $t^{-1/2}$, in agreement with a diffusional transport regime (see (II) in Fig. 4(B)). At around *t* = 70 s (see (III) in Fig. 4(B)), as the liposome moved closer to the electrode surface, the ECL intensity increased, in line with an increased local concentration of ECL reagents. Shortly before *t* = 80 s (see (IV) in Fig. 4(B)), the light intensity strongly decreased, corresponding to membrane permeabilization followed by dilution of ECL reagents. Finally, a further increase in ECL intensity was observed between 85 and 105 seconds (see (V) in Fig. 4(B)), due to diffusion of the luminophore and co-reactant from the more concentrated to the less concentrated area.

In the second case (i.e., ROI = white dotted circle – Fig. 4(C)), the same global behavior as that observed in Fig. 4(B) was obtained. However, the ECL increase is more important for the phase (III) in the local ROI of Fig. 3(C) compared to the global ROI of Fig. 3(B) because the liposome approaches the electrode surface and induces first higher local convection of the ECL reagents. In addition, we do not observe the re-increase in ECL intensity between 85 and 105 seconds (compare (V) in Figs. 4(C) and 4(B)). This was expected since even if diffusion of ECL reagents occurs, electron transfer cannot be achieved where phospholipids are blocking the electrode surface. We can also see that the increase in ECL intensity around 70 s is more marked when taking a ROI zone centered around the liposome (compare (III) in Figs. 4(C) and 4(B)). Note, at around *t* = 40 s, a slight increase of the ECL intensity was observed. This is again due to the local increase of concentration of

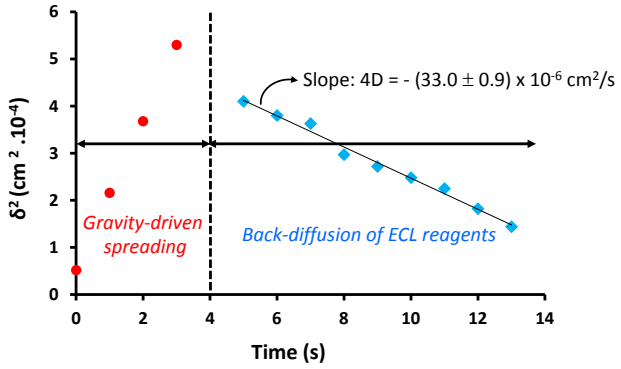

the ruthenium complex consecutive to convection in the solution caused by the arrival of other liposomes close to the investigated zone.

Characterization of the encapsulated solution dispersion and reagent diffusion in SECL.

Based on the results reported in the previous section, it was possible to observe not only the dispersion of the released solution, but also the diffusion of the ECL reagents from the bulk (the area with the highest luminophore concentration) to the released solution region (the zone with the lowest luminophore concentration). Considering that the diffusion layer thickness is proportional to $2(Dt)^{1/2}$, the evolution of the square of the apparent expansion distance (δ^2) of the black spot was plotted as a function of time (Fig. 5). In this Figure, the moment when the liposome begins to leak/permeabilize is defined as t = 0 s. Two opposite slopes (increasing then decreasing) are observed, indicating a change in the direction

of propagation of the black spot that can be explained by a change in the transport mode of the ECL reagents. Accordingly, as already observed in positive ECL,[17] at short time scale (see red dots in Fig. 5), the release of solution following contact with the polarized electrode surface induces the expansion of the non-emitting ECL area. The opening event generates a gravity-driven spreading, notably under the effect of the density difference between glucose (extra-vesicular solution) and sucrose (intra-vesicular solution). It is noteworthy that the gravity-driven spreading of the vesicle content exhibits a diffusive behavior (δ^2 proportional to time). This time dependence has already been observed for a liquid sessile drop spreading in another miscible liquid and was attributed to the diffusion of momentum.[89] A diffuse layer forms at the drop surface and drains due to decreasing viscosity.

At longer times, represented by the blue squares, the decrease accounts for the back-diffusion of ECL reagents to the less concentrated region. In other words, it corresponds to the decrease of the non-emitting ECL region. The value of this slope (i.e., 4D) is in keeping with that expected for a bidimensional mean square displacement ($\delta^2 = 4Dt$) of small molecules by diffusion, giving a value D = (8.3 ± 0.9) x 10^{-6} cm^2/s. This value is similar to the previously reported value of D for $[Ru(bpy)_3]^{2+}$ of 5.9 x 10^{-6} cm^2/s[90, 91] and validates our SECL approach.

Fig. 5 Evolution of the square of the apparent distance of propagation (δ^2) of the black spot (i.e. non-emitting ECL area) as a function of time. At t > 4 s, the diffusion coefficient D ((8.3 ± 0.9) x 10^{-6} cm^2/s) was estimated from the slope (4D) of the linear fitting function (blue squares). This figure was obtained after treatment of images recorded for the liposome shown in Fig. 4. Note: in this Figure t = 0 s is defined as the moment when the liposome begins to leak/permeabilize. Diffusion regime line equation: $\delta^2 = -0.33\ t + 5.78$ ($R^2 = 0.989$). t = 0 s corresponds to the time at which the liposome started to release its content.

Conclusions

Herein, we have shown that the permeabilization of giant liposomes can be imaged by shadow ECL (SECL) microscopy. Compared with the positive ECL approach, SECL does not require encapsulation of ECL reagents inside the liposomes. Although based on opposite modalities, positive and negative (shadow) ECL provide convergent and complementary information on the permeabilization/opening of liposomes, namely: (i) membrane rupture occurs when liposomes are in contact with the surface of a polarized electrode; (ii) the brutal rupture of the membrane causes convection leading to rapid dilution of the ECL reagents; (iii) a diffusion regime subsequently sets in after a few seconds to compensate the concentration gradients generated by convection. Finally, SECL and ECL appear complementary to assess liposome integrity as well as to characterize permeabilization events, a central issue in molecule release or delivery.

Author Contributions

All authors contributed to the study conception, design, and analysis. The manuscript was written through contributions of all authors. All authors have given approval to the final version of the manuscript

Conflicts of interest

There are no conflicts to declare.

Acknowledgements

This work was supported in parts by CNRS UMR 8640, Ecole Normale Supérieure, PSL University and Sorbonne Université. F.B.T. thanks the doctoral school ED388 “Chimie Physique et de Chimie Analytique de Paris Centre” for a PhD grant. N.S. acknowledges the financial support from Agence Nationale de la Recherche (ELISE - ANR-21-CE42).

References

1 N.J. Yang and M.J. Hinner, (2015). *Getting Across the Cell Membrane: An Overview for Small Molecules, Peptides, and Proteins*. In: A. Gautier and M. Hinner (eds), *Site-Specific Protein Labeling. Methods in Molecular Biology*, vol. **1266**. Humana Press, New York, NY. https://doi.org/10.1007/978-1-4939-2272-7_3

2 J. Kulbacka, A. Choromańska, J. Rossowska, J. Weżgowiec, J. Saczko and M.P. Rols (2017). Cell Membrane Transport Mechanisms: Ion Channels and Electrical Properties of Cell Membranes. In: J. Kulbacka and S. Satkauskas (eds) Transport Across Natural and Modified Biological Membranes and its Implications in Physiology and Therapy. Advances in Anatomy, Embryology and Cell Biology, vol **227**. Springer, Cham. https://doi.org/10.1007/978-3-319-56895-9_3

3 C. Bechara and S. Sagan, *FEBS Lett*., 2013, **587**, 1693–1702.

4 E. Neher and B. Sakmann, In: Single-Channel Recording, 2nd Ed. (Plenum Press, New York and London, 1995). https://doi.org/10.1007/978-1-4419-1229-9

5 G. Nasr, H. Greige-Gerges, A. Elaissari and N. Khreich, *Int. J. Pharm*., 2020, **580**, 119198.

6 H. Zhang, H. Jiang, X. Liu and X. Wang, *Anal. Chim. Acta.,* 2024, **1285**, 341920.

7 C. Amatore, S. Arbault, M. Guille and F. Lemaître, *Chem Rev*., 2008, **108**, 2585-2621.

8 P. Lefrançois, J. Santolini and S. Arbault, *Anal Chem*., 2021, **93**, 13143–51.

9 P. Messina, F. Lemaitre, F. Huet, K.A. Ngo, V. Vivier, E. Labbé, O. Buriez and C. Amatore, *Angew Chem Int Ed.,* 2014, **53**, 3192–3196.

10 M. Guille-Collignon, J. Delacotte, F. Lemaître, E. Labbé and O. Buriez. *Chem. Rec*., 2021, **21**, 1–11.

11 M. Čížková, L. Cattiaux, J.M. Mallet, E. Labbé and O. Buriez, *Electrochim. Acta*., 2018, **260**, 589-597.

12 M. Čížková, L. Cattiaux, J. Pandard, M. Guille-Collignon, F. Lemaitre, J. Delacotte, J.M. Mallet, E. Labbé and O. Buriez, *Electrochem. Commun*., 2018, **97**, 46-50.

13 R. De Oliveira, M. Durand, L. Challier, P. Messina, J.M. Swiecicki, M. Di Pisa, G. Chassaing, S. Lavielle, O. Buriez and E. Labbé, *J. Electroanal. Chem.*, 2017, **788**, 225-231.

14 X. Liu, A. Savy, S. Maurin, L. Grimaud, F. Darchen, D. Quinton, E. Labbé, O. Buriez, J. Delacotte, F. Lemaître and M. Guille-Collignon, *Angew Chem Int Ed Engl*., 2017, **56**, 2366-2370.
15 L. Li, Y. Chen and J.J. Zhu, *Anal. Chem.,* 2017, **89**, 358-371.
16 C. Ma, Y. Cao, X. Gou and J.J. Zhu, *Anal. Chem.,* 2020, **92**, 431-454.
17 F. Ben Trad, V. Wieczny, J. Delacotte, M. Morel, M. Guille-Collignon, S. Arbault, F. Lemaitre, N. Sojic, E. Labbé and O. Buriez, *Anal Chem*., 2022, **94**, 1686–1696.
18 F. Ben Trad, J. Delacotte, M. Guille-Collignon, F. Lemaitre, S. Arbault, N. Sojic, F. Burlina, E. Labbé and O. Buriez, *Chem Biomed Imaging*., 2023, **1**, 58–65.
19 V.P. Torchilin, *Nat. Rev. Drug Discov.*, 2005, **4**, 145−160.
20 T.M. Allen and P.R. Cullis, *Adv. Drug Deliv. Rev.*, 2013, **65**, 36–48.
21 B.S. Pattni, V.V. Chupin and V.P. Torchilin, *Chem. Rev*., 2015, **115**, 10938−10966. New Developments in Liposomal Drug Delivery.
22 V. Noireaux and A.A. Libchaber, *Proc. Natl. Acad. Sci. U. S. A*., 2004, **101**, 17669−17674.
23 S.S. Mansy, J.P. Schrum, M. Krishnamurthy, S. Tobe, D.A. Treco and J.W. Szostak, *Nature,* 2008, **454**, 122−125.
24 P.Y. Bolinger, D. Stamou and H. Vogel, *J. Am. Chem. Soc*., 2004, **126**, 8594−8595.
25 J. Zimmerberg and M.M. Kozlov, *Nat. Rev. Mol. Cell Biol*., 2006, **7**, 9−19.
26 A.D. Bangham, M.W. Hill and N.G.A. Miller, In *Methods in Membrane Biology*; E.D. Korn, Ed.; Springer US: Boston, MA, 1974; Vol. 1, pp 1−68.
27 V. Früh, A.P. IJzerman and G. Siegal, *Chem. Rev*., 2011, **111**, 640−656.
28 K. Adamala and J.W. Szostak, *Science*, 2013, **342**, 1098−1100.
29 H. Saito, Y. Kato, M. Le Berre, A. Yamada, T. Inoue, K. Yosikawa and D. Baigl, *ChemBioChem.*, 2009, **10**, 1640−1643.
30 J.W. Szostak, D.P. Bartel and P.L. Luisi, *Nature*, 2001, **409**, 387−390.
31 K. Kurihara, Y. Okura, M. Matsuo, T. Toyota, K. Suzuki and T. Sugawara, *Nat. Commun*., 2015, **6**, 8352.
32 M. Osawa and H.P. Erickson, *Proc. Natl. Acad. Sci. U. S. A*., 2013, **110**, 11000−11004.
33 S. Deshpande, Y. Caspi, A.E.C. Meijering and C. Dekker, *Nat. Commun*., 2016, **7**, 10447.
34 R. Dimova, *Annu. Rev. Biophys*., 2019, **48**, 93−119.
35 I.L. Jørgensen, G.C. Kemmer and T.G. Pomorski, *Eur. Biophys. J*., 2017, **46**, 103−119.
36 T. Robinson, *Adv. Biosyst*. 2019, **3**, 1800318.
37 S. Matosevic, Bioessays, 2012, **34**, 992−1001.
38 C. Ma, S. Wu, Y. Zhou, H.-F. Wei, J. Zhang, Z. Chen, J.J. Zhu, Y. Lin and W. Zhu, *Angew. Chem. Int. Ed.,* 2021, **60**, 4907-4914.
39 X. Gou, Z. Xing, C. Ma and J.J. Zhu, *Chem. Biomed. Imaging,* 2023, **1**, 414–433.
40 X. Ma, W. Gao, F. Du, F. Yuan, J. Yu, Y. Guan, N. Sojic and G. Xu. *Acc Chem Res.*, 2021, **54**, 2936-2945.
41 A. Fiorani, D. Han, D. Jiang, D. Fang, F. Paolucci, N. Sojic and G. Valenti, *Chem Sci*., 2020, **11**, 10496−10500.
42 A. Zanut, F. Palomba, M. Rossi Scota, S. Rebeccani, M. Marcaccio, D. Genovese, E. Rampazzo, G. Valenti, F. Paolucci and L. Prodi, *Angew Chem Int Ed*., 2020, **59**, 21858−21863.
43 F. Du, Y. Chen, C. Meng, B. Lou, W. Zhang and G. Xu, *Curr. Opin. Electrochem.*, 2021, **28**, 100725.
44 P. Dutta, D. Han, B. Goudeau, D. Jiang, D. Fang and N. Sojic, *Biosens Bioelectron*., 2020, **165**, 112372.
45 J. Zhang, S. Arbault, N. Sojic and D. Jiang, *Annu. Rev. Anal. Chem*., 2019, **12**, 275-295.
46 S. Rebeccani, A. Zanut, C.I. Santo, G. Valenti and F. Paolucci, *Anal Chem*., 2022, **94**, 336-348.
47 W. Zhao, H.Y. Chen and J.J. Xu, *Chem Sci*., 2021, **12**, 5720-5736.
48 Y. Lu, X. Huang, S. Wang, B. Li and B. Liu, *ACS Nano,* 2023, **17**, 3809–3817.
49 Y. Liu, Y. Yao, B. Yang, Y.J. Liu and B. Liu, *Chinese Chemical Letters,* 2022, **33**, 2705-2707.
50 Y. Lu, Y. Ning, B. Li and B. Liu, *Anal. Chem.,* 2024, **96**, 463-470.
51 J.E. Dick, C. Renault, B.K. Kim, A.J. Bard, *Angew. Chem. Int. Ed*., 2014, **53**, 11859−11862.
52 B.R. Layman and J.E. Dick, *J. Am. Chem*. Soc. 2024, **146**, 707–713.
53 J. Dong, Y. Lu, Y. Xu, F. Chen, J. Yang, Y. Chen and J. Feng, *Nature*, 2021, **596**, 244-249.
54 J. Dong, Y. Xu, Z. Zhang and J. Feng, *Angew. Chem. Int. Ed*., 2022, **61**, e202200187.
55 L. Xu, Y. Li, S. Wu, X. Liu and B. Su, *Angew. Chem. Int. Ed*., 2012, **51**, 8068-8072.
56 M.J. Zhu, J.B. Pan, Z.Q. Wu, X.Y. Gao, W. Zhao, X.H. Xia, J.J. Xu and H.Y. Chen, *Angew. Chem. Int. Ed*., 2018, **57**, 4010−4014.
57 C. Ma, X. Gou, Z. Xing, M.X. Wang, W. Zhu, Q. Xu, D. Jiang and J.J. Zhu, *Research,* 2023, **6**, 0257.
58 C. Ma, W. Wu, L. Li, S. Wu, J. Zhang, Z. Chen and J.J. Zhu, *Chem. Sci.,* 2018, **9**, 6167-6175.
59 M. Sentic, M. Milutinovic, F. Kanoufi, D. Manojlovic, S. Arbault and N. Sojic, *Chem. Sci.*, 2014, **5**, 2568−2572.
60 F. Deiss, C.N. LaFratta, M. Symer, T.M. Blicharz, N. Sojic and D.R. Walt, *J. Am. Chem. Soc.*, 2009, **131**, 6088−6089.
61 G. Valenti, M. Zangheri, S.E. Sansaloni, M. Mirasoli, A. Penicaud, A. Roda and F. Paolucci, *Chem. Eur. J*., 2015, **21**, 12640−12645.
62 J. Xu, P. Huang, Y. Qin, D. Jiang and H.Y. Chen, *Anal. Chem*., 2016, **88**, 4609−4612.
63 G.Z. Ma, J.Y. Zhou, C.X. Tian, D.C. Jiang, D.J. Fang and H.Y. Chen, *Anal. Chem*., 2013, **85**, 3912−3917.
64 G. Liu, C. Ma, B.K. Jin, C.X. Chen and J.J. Zhu, *Anal. Chem*., 2018, **90**, 4801−4806.
65 S. Voci, B. Goudeau, G. Valenti, A. Lesch, M. Jović, S. Rapino, F. Paolucci, S. Arbault and N. Sojic, *J. Am. Chem. Soc*., 2018, **140**, 14753−14760.
66 L. Ding, P. Zhou, Y. Yan and B. Su, *Chem. Biomed. Imaging*, 2023, **1**, 558–565.
67 M. Guo, D. Du, J. Wang, Y. Ma, D. Yang, M.A. Haghighatbin, J. Shu, W. Nie, R. Zhang, Z. Bian, L. Wang, Z.J. Smith and H. Cui, *Chem. Biomed. Imaging*, 2023, **1**, 179–185.
68 Y. Liu, H. Zhang, B. Li, J. Liu, D. Jiang, B. Liu and N. Sojic, *J. Am. Chem. Soc.,* 2021, **143**, 17910-17914.
69 H. Xiong, Z. Huang, Q. Lin, B. Yang, F. Yan, B. Liu, H. Chen and J. Kong, *Anal. Chem.,* 2022, **94**, 837-846.
70 X. Gou, Y. Zhang, Z. Xing, C. Ma, C. Mao and J.J. Zhu, *Chem. Sci.,* 2023, **14**, 9074-9085.
71 H. Zhu, D. Jiang and J.J. Zhu, *Chem. Sci.* 2021, **12**, 4794−4799.
72 G. Valenti, S. Scarabino, B. Goudeau, A. Lesch, M. Jović, E. Villani, M. Sentic, S. Rapino, S. Arbault, F. Paolucci and N. Sojic, *J. Am. Chem. Soc.,* 2017, 139, 16830−16837.
73 A.J. Wilson, K. Marchuk and K.A. Willets, *Nano Lett.,* 2015, **15**, 6110−6115.
74 J. Zhou, G. Ma, Y. Chen, D. Fang, D. Jiang and H. Chen, *Anal. Chem.,* 2015, **87**, 8138−8143.
75 Y. Chen, D. Zhao, J. Fu, X. Gou, D. Jiang, H. Dong and J.J. Zhu, *Anal. Chem.,* 2019, **91**, 6829−6835.

76 F. Ben Trad, B. Carré, J. Delacotte, F. Lemaître, M. Guille-Collignon, S. Arbault, N. Sojic, E. Labbé and O. Buriez, *Anal. Bioanal. Chem*., 2024 Jan 16. doi: 10.1007/s00216-024-05133-y. Epub ahead of print. PMID: 38227016.
77 L. Xu, Z. Zhou, C. Zhang, Y. He and B. Su, *Chem. Commun.* 2014, **50**, 9097−9100.
78 H. Ding, P. Zhou, W. Fu, L. Ding, W. Guo and B. Su, *Angew. Chem., Int. Ed.* 2021, **60**, 11769−11773.
79 Y. Ma, C. Colin, J. Descamps, S. Arbault and N. Sojic, *Angew. Chem., Int. Ed.* 2021, **60**, 18742−18749.
80 A. Zanut, A. Fiorani, S. Canola, T. Saito, N. Ziebart, S. Rapino, S. Rebeccani, A. Barbon, T. Irie, H.P. Josel, F. Negri, M. Marcaccio, M. Windfuhr, K. Imai, G. Valenti and F. Paolucci, *Nat. Commun.,* 2020, **11**, 2668.
81 S. Knezevic, E. Kerr, B. Goudeau, G. Valenti, F. Paolucci, P.S. Francis, F. Kanoufi and N. Sojic, *Anal. Chem*., 2023, **95**, 7372−7378.
82 J. Tan, L. Xu, T. Li, B. Su and J. Wu, *Angew. Chem., Int. Ed*., 2014, **53**, 9822-9826.
83 J. Dong and J. Feng, *Anal. Chem*. 2023, **95**, 374-387.
84 C.A. Schneider, W.S. Rasband and K.W. Eliceiri, *Nat. Methods*, 2012, **9**, 671–675.
85 Y. Wang, W. Guo, Q. Yang, B. Su, *J. Am. Chem. Soc*. 2020, **142**, 1222-1226.
86 W.-X. Fu, P. Zhou, W. Guo, B. Su, *Adv. Sens. Energy Mater*., 2022, **1**, 100028.
87 S. Rebeccani, A. Zanut, C. I. Santo, G. Valenti, F. Paolucci, *Anal. Chem*. 2021, **94**, 336-348.
88 W. Guo, P. Zhou, L. Sun, H. Ding, B. Su, *Angew. Chem., Int. Ed*., 2021, **60**, 2089-2093.
89 D.J. Walls, E. Meiburg and G.G. Fuller, *J. Fluid Mech*., 2018, **852**, 422–452
90 C. Amatore, A. Chovin, P. Garrigue, L. Servant, N. Sojic, S. Szunerits and L. Thouin, *Anal. Chem*., 2004, **76**, 7202-7210.
91 Y. Zu, Z. Ding, J. Zhou, Y. Lee and A. J. Bard, *Anal. Chem*., 2001, **73**, 2153-2156.